RESEARCH ARTICLE

ADVANCED
NANOBIOMED
RESEARCH
Open Access

www.advnanobiomedres.com

Integrin α$_{IIb}$β$_3$ Activation and Clustering in Minimal Synthetic Cells

Lucia T. Benk, Amelie S. Benk, Rafael B. Lira, Elisabetta Ada Cavalcanti-Adam, Rumiana Dimova, Reinhard Lipowsky, Benjamin Geiger, and Joachim P. Spatz*

Platelet adhesion and activation are mediated by integrin α$_{IIb}$β$_3$ clustering, which is crucial for the hemostatic function of platelets. In an activated state, integrins provide the connection between the extracellular matrix and the actin cytoskeleton through a variety of cytoplasmic proteins, such as talin. Here, droplet-based microfluidics is applied to generate cell-sized giant unilamellar vesicles (GUVs) with a defined molecular composition to quantify the adhesion of integrin α$_{IIb}$β$_3$-containing protocells in relation to the number of integrin–talin head domain (THD) complexes. Furthermore, it is shown that THD induces integrin clustering in protocells adhering to fibrinogen. The formation of this molecular link, which has, so far, only been observed in vivo, is an essential step in synthetic cell design to recapitulate integrin-mediated bidirectional signaling across the membrane. These results pave the way for further quantitative investigations of protein–protein interactions between integrins and associated proteins and their assembly within such defined, but complex, synthetic cells. An essential future step to mimic the complex interaction between cells and their environment will be to combine synthetic approaches with peptide chemistry to guide the molecular mechanisms involved in integrin binding and activation.

1. Introduction

In multicellular organisms, cell adhesion to the extracellular matrix (ECM) plays an essential role in many processes regulating cell survival, proliferation, morphogenesis, tissue hemostasis, wound healing, and tumorigenesis.[1] Integrins are heterodimeric transmembrane receptors that bind to specific sequences present in ECM proteins and mediate cell–ECM physical interactions and mechanical signaling at focal adhesions.[1b,2] Here, a dynamic network of cytoplasmic proteins, recruited upon integrin lateral clustering, mediates the connection of the actin cytoskeleton to specific ECM components.[1a,2c,2d,3] For integrin clustering, integrin activation, ligand binding, and lateral diffusion are required.[1,2d,4]

The integrin family is consisting of 24 different heterodimeric members, which are grouped into 8 subgroups depending on their β subunit.[5c] In platelets, integrin α$_{IIb}$β$_3$ is the dominant receptor at the cell membrane and it is crucial for platelet function in hemostasis and thrombosis. The initial adhesive interactions between integrin α$_{IIb}$β$_3$ and fibrinogen activate kinase-mediated signaling and cytoskeletal organization, resulting in the formation of focal adhesion-like structures and generation of forces.

The use of biomimetic ligands with high-affinity integrin α$_{IIb}$β$_3$[6] and immobilized on nanopatterned surfaces to control binding sites[7] has revealed the importance of integrin α$_{IIb}$β$_3$ clustering in the local regulation of platelet adhesion. Platelets exhibit a distinct mode of sensing ligand density, where filopodia are formed up to 100 nm ligand spacing, but stable adhesions comparable to the ones formed on fibrinogen, are observed for ligand spacing up to 60 nm. Surprisingly, the

---

L. T. Benk, A. S. Benk, E. A. Cavalcanti-Adam, J. P. Spatz
Department of Cellular Biophysics
Max Planck Institute for Medical Research
Jahnstr. 29, 69120 Heidelberg, Germany
E-mail: spatz@mr.mpg.de

R. B. Lira, R. Dimova, R. Lipowsky
Theory & Bio-Systems
Max Planck Institute of Colloids and Interfaces
14424 Potsdam, Germany

R. B. Lira
Faculty of Science and Engineering
Molecular Biophysics
Zernike Institute for Advanced Materials
9747 AG Groningen, The Netherlands

E. A. Cavalcanti-Adam, R. Lipowsky, J. P. Spatz
Max Planck School Matter to Life
Jahnstr. 29, 69120 Heidelberg, Germany

B. Geiger
Department of Molecular Cell Biology
Weizmann Institute of Science
Rehovot 76100, Israel

J. P. Spatz
Institute for Molecular Systems Engineering (IMSE)
Heidelberg University
69120 Heidelberg, Germany

**ADVANCED
SCIENCE NEWS**
www.advancedsciencenews.com

**ADVANCED
NANOBIOMED
RESEARCH**
Open Access

www.advnanobiomedres.com

platelets could still attach at 120 nm spacing, although filopodia could not be observed. This study suggests that integrin $\alpha_{IIb}\beta_3$ activation is responsible for the local adhesion to the surface, and that for the stability of adhesion further molecular interactions regulate the global adhesion process.

On the surface of platelets, integrin $\alpha_{IIb}\beta_3$ is present in a bent and inactive state and becomes activated through high-affinity interactions with its ligands, such as fibrinogen.[5] Integrin conformational change is induced either by divalent cations like Mn^{2+} in the extracellular environment or by intracellular proteins involved in the so-called inside–out signaling.[3b,5c,8] One of these cytoplasmic proteins is talin, a key player in integrin activation by directly linking the integrin's cytoplasmic tail with the actin cytoskeleton.[3b,9] Additionally, talin has a proven role in the formation of integrin clusters which provide dynamic links and bidirectional signaling between the intracellular and the extracellular environments.[1b,2d,10] Loss of talin1 impairs activation of integrin $\alpha_{IIb}\beta_3$ in platelets and adhesion to ECM proteins.[11]

The role of the talin head domain (THD), which directly binds to integrin cytoplasmic tail, in activation and clustering of integrin has been mainly investigated by the top-down approach in cell-based studies, using overexpression or knockdown strategies.[2d,9c,9e,12] Such in vivo models are valuable tools for understanding focal adhesion assembly. However, they entail technical limitations, as only a restricted number of exogenous components can be successfully inserted into a living cell and their insertion might disturb the natural processes of the cell. In general, in vivo studies always include unknown parameters within the cellular environment that are likely to reduce the precision of the observations.[5b]

Consequently, in vitro models have been applied to overcome those limitations.[9a] The controlled insertion of the desired components into the system allows for a more quantitative analysis of the events at focal adhesion sites.[5b] One strategy to reconstruct THD-induced integrin activation in vitro is based on utilizing large unilamellar vesicles (LUVs).[9a] The THD-enclosing integrin-liposomes are produced by combining lipids, integrin, and THD in the presence of a detergent that is subsequently removed. On account of the purity of the system, it was possible to measure flow cytometrically that THD activates integrin independently of supporting co-factors.[9a] Another way is the insertion of single integrin molecules into phospholipid nanodiscs. THD introduced to the system at a known concentration can bind to integrin and induce an increase in affinity, which is detectable by enzyme-linked immunoabsorbent assay (ELISA). These observations confirm that pure THD is sufficient for activating integrin.[9a] However, both in vitro models are far from being able to mimic the cellular environment. For example, LUVs (100–1000 nm) provide a lipid compartment similar to the cellular membrane but have a much smaller interior volume and a larger radius of curvature. Thus, the encapsulated amount of THD is difficult to predict and, in particular, concentrations quickly change during the experiment, making studies in the equilibrium impossible. Additionally, so far, no integrin clustering induced by THD has been observed in vitro.

In this study, we modified a recently published, droplet-based microfluidic technique to create integrin- and THD-containing synthetic cells as a minimal approach to fundamentally identify

key regulators in integrin $\alpha_{IIb}\beta_3$ clustering.[13] The protocells were formed by encapsulating bare LUVs, integrin-containing liposomes, and THD into monodisperse water-in-oil droplets stabilized by block-copolymers (**Figure 1**a,I). In each droplet, the liposomes adsorb, rupture, and fuse at the inner interface, forming "droplet-stabilized giant unilamellar vesicles" (dsGUVs) as a result (Figure 1a,II). Subsequently, the protocells were released from the oil phase into a physiologically relevant environment to perform adhesion studies (Figure 1a,III–V).

This method allows for the quantitatively precise loading of giant unilamellar lipid vesicles (GUVs) with transmembrane and cytoplasmic proteins to mimic and analyze cellular functions. Here, we demonstrate for the first time the activation and clustering of integrin $\alpha_{IIb}\beta_3$ in cell-sized GUVs—induced by THD and controlled by the quantitative THD:integrin ratio. In addition, the adhesion of vesicles as it correlates to the integrin–THD complex density was investigated.

2. Results and Discussion

2.1. Formation of Cationic GUVs Containing Integrin $\alpha_{IIb}\beta_3$ and THD Complexes

To investigate the role of THD in integrin-mediated adhesion and integrin clustering in vitro, cell-sized integrin-liposomes enclosing THD were produced by droplet-based microfluidics. The original technique, developed by Weiss et al.,[13] required the addition of 10 mM Mg^{2+} to the system as a mediator for charge-driven adhesion of negatively charged lipids on the inner droplets' interface.[13] Thus, the protocol could not be used to investigate THD-induced activation, because divalent cations, especially Mn^{2+} but also Mg^{2+}, can activate integrins.[5c,8] Therefore, in the present study, we developed a protocol in which positively charged lipids that are integrated into LUVs will induce charge-mediated attraction with the negatively charged droplet inner interface. GUVs with a cationic lipid fraction of 5–80 mol% without the need to add other cations were formed (Supplementary Methods, Figure S3, Supporting Information).

Fluorescence recovery after photobleaching (FRAP), fluctuation and intensity analyses of the released cationic GUVs indicate that the lipid membrane is free of traces of the oil phase and that the released GUVs are intact and their content is preserved without leakage into the surrounding solution (Supplementary Methods, Figure S4, Supporting Information), which is in agreement with Weiss et al.[13] The availability of protocells formed via droplet-based microfluidics and free of divalent cations allows for synthetic cell applications that were not possible in the past. However, it has to be kept in mind that natural cellular membranes exhibit an overall negative charge. The membrane charge plays an important role in some protein interactions in vivo. For example, the F1 and F2 subdomain of THD present a positively charged patch that is supposed to interact with the negatively charged cell membrane.[12a] It is assumed that this interaction helps to establish the orientation of THD.[9b,12a] In our system, the conditions for this interaction are not given.

The formation of positively charged GUVs using standard methods, especially bulk methods, has been challenging in the past. Here, we introduce a method for the production of
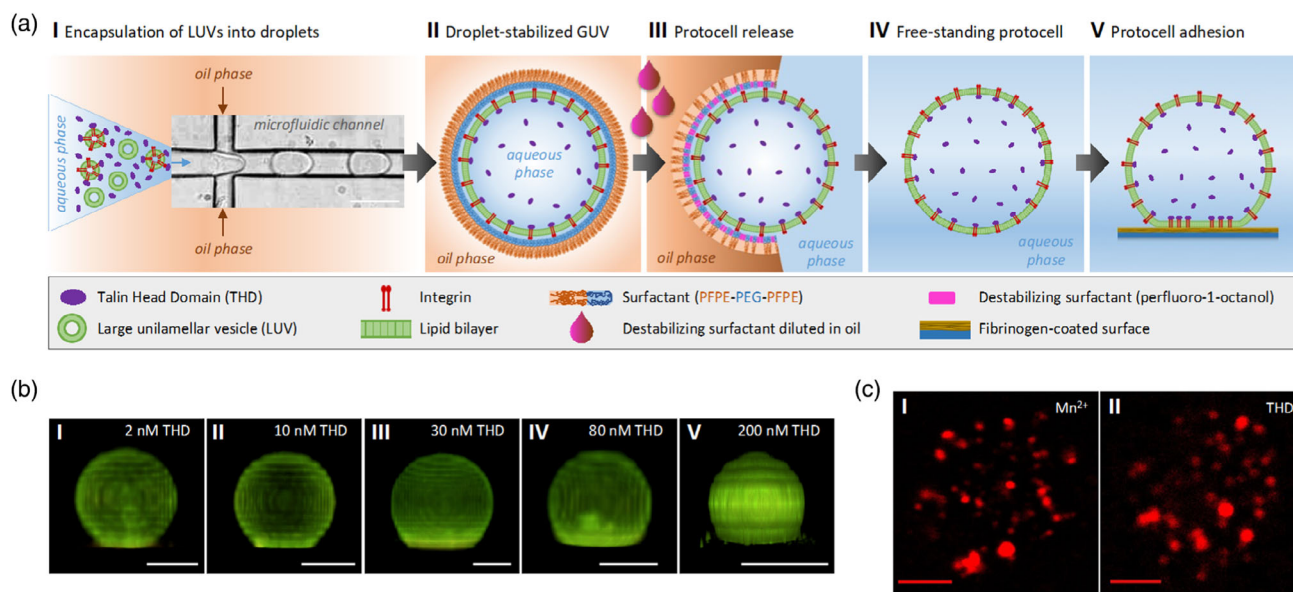
ADVANCED
SCIENCE NEWS

www.advancedsciencenews.com

ADVANCED
NANOBIOMED
RESEARCH
Open Access

www.advnanobiomedres.com

Figure 1. Formation and adhesion of protocells containing integrin and THD. a) Schematic depiction of the formation of functional cell-sized liposomes that contain integrin and THD by droplet-based microfluidics. Scale bar: 50 μm. I) Encapsulation of bare liposomes (≈100 nm diameter), integrin-reconstituted proteoliposomes, and THD at defined concentration into microfluidic water-in-oil droplets of 30 μm diameter. II) Liposomes rupture at the droplets' inner interface, fuse, and form a continuous lipid bilayer, the dsGUV. III) After the addition of destabilizing surfactant, the GUV is released from the stabilizing oil phase into an aqueous phase, i.e., an appropriate buffer solution. IV) Free-standing GUV that contains integrin and THD of defined concentrations, after its release. V) Released GUV adhering to a fibrinogen-coated surface as a result of integrin-activation by THD. Depiction not to scale. b) 3D-reconstitutions of integrin-containing protocells (lipid: ATTO488 (green), integrin: Alexa568 (red)). The images show increasing adhesion to fibrinogen-coated surfaces in correlation to an initially provided THD concentration of: I) 2 nM, II) 10 nM, III) 30 nM, IV) 80 nM, V) 200 nM at a constant integrin concentration. The spreading value of each vesicle shown is close to the mean value obtained from a corresponding sample of vesicles. For correlating data refer to Table 1. Scale bar: 10 μm. c) Integrin-clustering in the contact area of protocells adhering to fibrinogen-coated surfaces. The lipid composition of the protocells is 18:72:10 DOTAP:DOPC:Egg PC with reconstituted integrin (Alexa568) activated by: I) 1 mM Mn^{2+}/1 mM Mg^{2+} (vesicle diameter: 12 μm) and II) 200 nM THD (vesicle diameter: 14 μm). The difference in the overall signal and concentration of clusters can be due to bleaching effects. Scale bar: 3 μm.

monodisperse cationic GUVs at high throughput (Figure S3, Supporting Information). As an additional feature, we can endow the cationic GUVs with transmembrane proteins or encapsulate defined amounts of components. So far, cationic liposomes have mainly played a role in charge-driven membrane fusion.[14] With our approach, we are able to create protocells that contain a defined amount of THD and integrin $\alpha_{IIb}\beta_3$ molecules in an environment free of divalent cations.

2.2. THD Induces Integrin $\alpha_{IIb}\beta_3$ Clustering and Adhesion of Integrin-Reconstituted Protocells

We next determined the THD-induced activation and clustering of integrin $\alpha_{IIb}\beta_3$ in cell-sized liposomes adhering to fibrinogen-coated surfaces. Here, the adhesion of the vesicles correlates with the initially provided concentrations of THD and integrin (Figure 1b).

2.3. Quantification of Integrin, THD, and Integrin–THD Complexes within the Protocell

It is assumed that integrin–THD complex formation follows the Langmuir adsorption model

$$\frac{KM_T}{1 + KM_T} = \frac{M_{I\uparrow T}}{\frac{1}{2}N_I} \tag{1}$$

where M_T denotes the concentration of THD in solution, N_I the density of reconstituted integrin and $M_{I\uparrow T}$ the integrin–THD complex density. Moreover, it is assumed that reconstituted integrin proteins are randomly oriented either to the inside or to the outside of the liposome. Therefore, only 50% of them present their cytoplasmic domain to the side where they are accessible for ligand binding and the formation of integrin–THD complexes.[5b,15] The Langmuir adsorption constant K is the inverse of the dissociation constant K_d of the integrin–THD complex, which according to Yan et al. is assumed to be ≈100 nM for the binding of THD to the integrin β3 domain.[16]

The amount of THD, integrin, and integrin–THD complexes in the interior of the resulting protocells is calculated in two steps. In step 1, after bare LUVs, proteo-liposomes and THD are combined (Figure 1a,I, left side), the mass action equilibrium is evaluated for the first time, taking into account that the initial concentration M_T of THD in solution is reduced by the amount of THD that has been adsorbed by integrin

$$M_T = N_T - \gamma M_{I\uparrow T}^{LUV} \tag{2}$$

$M_{I\uparrow T}^{LUV}$ is the density of integrin–THD complexes and it is the average over the surface of all LUVs in liquid. The factor γ, defined as

$$\gamma = \frac{A_{GUV}}{N_A * V_{GUV}} \tag{3}$$

converts the molecular density $M_{I\uparrow T}^{LUV}$ into a molar concentration, in correspondence to Equation (1).

When the LUVs open up to create the supported lipid bilayer of the dsGUV (Figure 1a,II), the original orientation of integrin in the proteo-liposomes is conserved[15b] and either the inner or the outer leaflet of the LUV membranes adhere to the supporting surface.[17] It is assumed that both happen with equal probability, with the result that half of the preformed integrin–THD complexes have the desired orientation, i.e., THD is facing the inside of dsGUV, while the other half is oriented in the opposite direction.

In step 2 of the calculation, the mass action equilibrium is rebalanced within the dsGUVs. At this stage of the process, the initial concentration N_T of THD is reduced by the amount of THD that is bound to integrin at the inner side of the dsGUV membrane and the amount that is trapped outside

$$M_T^{GUV} = N_T - \gamma\left(M_{I\uparrow T}^{GUV} + \frac{1}{2} M_{I\uparrow T}^{LUV} \right) \tag{4}$$

The density $M_{I\uparrow T}^{GUV}$ of integrin–THD complexes with THD bound to the inner side of the dsGUV membrane is, therefore, given by

$$M_{I\uparrow T}^{GUV} = \frac{\left(\frac{1}{2}N_I + \frac{1}{\gamma}N_T - \frac{1}{2}M_{I\uparrow T}^{LUV} + \frac{K_d}{\gamma}\right) - \sqrt{\left(\frac{1}{2}N_I + \frac{1}{\gamma}N_T - \frac{1}{2}M_{I\uparrow T}^{LUV} + \frac{K_d}{\gamma}\right)^2 - 2N_I\left(\frac{1}{\gamma}N_T - \frac{1}{2}M_{I\uparrow T}^{LUV}\right)}}{2} \tag{5}$$

with

$$M_{I\uparrow T}^{LUV} = \frac{\left(\frac{1}{2}N_I + \frac{1}{\gamma}N_T + \frac{K_d}{\gamma}\right) - \sqrt{\left(\frac{1}{2}N_I + \frac{1}{\gamma}N_T + \frac{K_d}{\gamma}\right)^2 - 2N_I\frac{1}{\gamma}N_T}}{2} \tag{6}$$

At the end of the process, the protocells are released from the stabilizing droplet and transferred into the appropriate buffer solution (Figure 1a,III,IV). The molar THD:integrin ratio within a protocell depends on the size of its volume and surface area, both of which can be determined by treating the cell like a sphere and measuring its diameter. The protocells tend to break into smaller vesicles during the release process, pipetting, and sample preparation. To determine the volume and surface of a sample of protocells, we have averaged the diameter over all protocells.

2.4. Deriving the Adhesion Energy from the Spreading Value of Adhering Protocells

A non-adhering GUV can be approximated by a sphere, which changes its shape after adhesion to form a spherical cap with a radius r and a circular contact area with radius r_{adh} (Figure S1a, Supporting Information).[18] Here, we use this model to calculate the relationship between the contact angle ϑ and the spreading value Ω, which we define by

$$\Omega = \frac{A_{adh}}{A} \tag{7}$$

where A_{adh} denotes the contact area and A the projected area of the vesicle. According to the geometric model (Figure S1a, Supporting Information), we obtain

$$\cos\vartheta = \sqrt{1 - \frac{A_{adh}}{A}} = \sqrt{1 - \Omega} \tag{8}$$

The Young–Dupré equation

$$W = \sigma(1 - \cos\vartheta) \tag{9}$$

allows us to calculate the adhesion energy per area unit W if the contact angle ϑ and the membrane tension σ are known.[19] Within the limits of the geometrical model, this equation can be rewritten in the form

$$W = \sigma\left(1 - \sqrt{1 - \Omega}\right) \tag{10}$$

To check the validity of this equation, the contact angle ϑ of protocells with known spreading value Ω was experimentally determined by analyzing the reflection interference contrast microscopy (RICM) images (Figure S1b, Supporting Information). The results (Figure S1c and Table S1, Supporting Information) match well with the relation (Equation (9)) and thereby justify the usage of the modified Young–Dupré equation (Equation (10)).

2.5. Determining the Adhesion Energy to Membrane Tension Ratio of Protocells

The adhesion energy to membrane tension ratio (W/σ) is given by the geometrical factor in the modified Young–Dupré equation (Equation (10)). To determine the spreading value of each vesicle, confocal z-stack images were analyzed by Fiji/ImageJ (Version: 2.0.0-rc-30/1.49t). First, the contact area A_{adh} of the vesicle on the substrate was determined (feature: "analyze particles"). Second, the vesicle diameter was measured to calculate the area of the profile A. Only vesicles with a circular horizontal cross-section were analyzed and contributed to the mean spreading value of each sample.

The adhesion energy to membrane tension ratio (W/σ ratio), and correspondingly the adhesion energy, increases with integrin–THD complex density (**Figure 2**). The W/σ ratio is derived from the measured spreading value (**Table 1**). Above the density of 66 integrin–THD complexes/μm^2, the W/σ ratio grows only slightly, approaching a saturation value at ≈ 0.3. The density of 66 integrin–THD complexes/μm^2 corresponds to the molar THD:integrin ratio of 1:1 in vesicles with a diameter
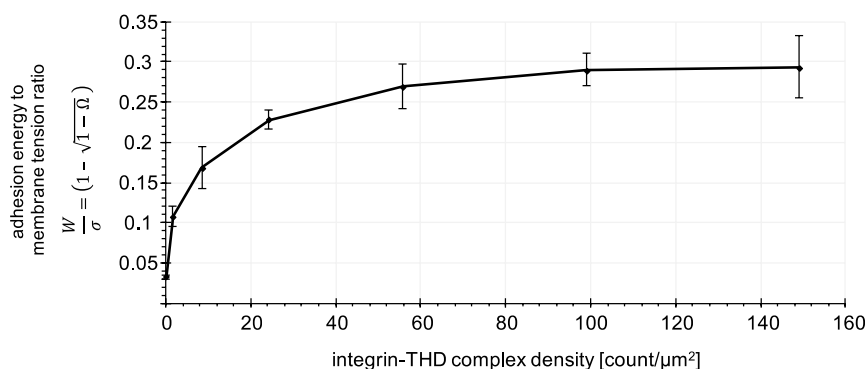
Figure 2. Mean adhesion energy (W) to membrane tension (σ) ratio (W/σ ratio) for integrin-containing protocells adhering to a fibrinogen-coated surface over the integrin–THD complex density. The graph is based on the values in Table 1. The error bars are calculated from the standard error of the mean spreading value.

Table 1. Properties of adhering integrin-containing protocells in relation to different THD concentrations. The initial THD concentration is the concentration supplied to create the protocells. The vesicle diameter is given by the mean value and its standard deviation. The integrin–THD complex density and the molar THD:integrin ratio is calculated using the K_d-value of integrin–THD complex formation of 100 nM.[13] The membrane of the protocells contains 330 integrin molecules/μm^2. Only integrins orientated with the extracellular domain to the outside of the vesicle (50%) contribute to the values in this table. The spreading value is given by the mean value and the standard error of the mean. The adhesion energy to membrane tension ratio (W/σ ratio) is derived from the spreading value Ω.

Initial THD concent-ration N_T [nM]	Number of analyzed vesicles	Vesicles diameter [μm]	THD-integrin complexes/μm^2	Molar THD:integrin ratio	Spreading value Ω	W/σ ratio
0	71	17.27 ± 4.35	0.00	0.00	0.064 ± 0.001	0.033 ± 0.003
2	40	16.16 ± 4.56	1.75	0.02	0.204 ± 0.0040	0.108 ± 0.013
10	33	15.09 ± 4.56	8.55	0.10	0.308 ± 0.007	0.168 + 0.03/−0.025
30	54	17.07 ± 6.46	24.28	0.33	0.404 ± 0.003	0.228 ± 0.012
80	32	15.88 ± 6.41	55.88	0.83	0.466 ± 0.007	0.269 + 0.028/−0.027
200	77	13.09 ± 4.80	99.01	1.79	0.495 ± 0.003	0.290 + 0.021/−0.020
1000	26	8.40 ± 1.90	148.91	5.63	0.500 ± 0.011	0.293 + 0.039/−0.037

of 15 μm. For comparison, in platelets, the proportion of THD to integrin is calculated to be in the range between 1:1 and 3:1.[9a]

As a positive control and for comparison, the mean spreading value Ω of integrin-containing protocells activated by Mn^{2+} and Mg^{2+} ions was measured to be 0.52 ± 0.043 ($W/\sigma = 0.31 ± 0.011$; number of analyzed vesicles: 15; mean diameter: 12.73 ± 4.7 μm; Figure S2III, Supporting Information). The value is close to the largest mean spreading value measured for THD-activated integrin-containing protocells (Table 1).

The negative controls show that there is no adhesion of THD-free integrin-reconstituted vesicles, and there is also no adhesion of vesicles containing THD or Mn^{2+}/Mg^{2+} but no integrin (Figure S2I, II, IV, Supporting Information). Nevertheless, the measured mean spreading value of the negative controls is not exactly zero, due to some few outliers. Furthermore, fluorescent patches of 0.3–0.6 μm in diameter are observed in the adhesive area of protocells containing Alexa568-labeled integrins, which are activated by THD ($N_T = 200$ nM) or Mn^{2+}/Mg^{2+} (Figure 1c). The patches indicate the formation of integrin clusters. Thereby, the ratio of the cluster to the adhesive area doesn't show any significant difference between integrin-containing GUVs activated by THD or Mn^{2+}/Mg^{2+} (Figure S5, Supporting Information). Figure S6, Supporting Information, shows control experiments to identify Mn^{2+}/Mg^{2+} or THD activation of integrins on fibrinogen-coated surfaces as a regulator for integrin cluster formation. Only mechanical formation of a contact to bovine serum albumin (BSA) as passivating layer did not result in integrin cluster formation.

The Young–Dupré equation (Equation (10)) relates the contact angle of adhering vesicles to its adhesion energy and membrane tension.[18] A geometric model[18] is used to derive the contact angle of the vesicle in good approximation (Equation (7,8)). This is confirmed by evaluating RICM images of adhering vesicles with known spreading value.[20]

The relatively high dispersion of the spreading value within each sample can be an effect of varying membrane tensions of the vesicles. Within the same sample, vesicles with low membrane tension have a larger adhesion area than tense vesicles with a higher membrane tension which may be caused by variations in integrin distributions. Therefore, the spreading value can vary within the same sample of GUVs. The spreading value

was measured in several independently performed experiments, which provided similar mean values. A high variance in adhesion-induced vesicle deformation has been also observed by Gleisner et al.[18]

3. Conclusion and Perspective

In this study, the activating role of THD in the integrin-mediated adhesion process was investigated in vitro. To this purpose, cell-sized liposomes functionalized with integrin $\alpha_{IIb}\beta_3$ and THD were created by droplet-based microfluidics (Figure 1a). The approach allows for the formation of complex synthetic cells with defined constituents. Here, the molecular density of integrin–THD complexes in the vesicle membrane was adjusted. The adhesion of the vesicles to a fibrinogen-coated surface was investigated by measuring their spreading value Ω, which is a geometrical property defined in this article. We verified that the spreading value can be used in a modified version (Equation (10)) of the Young–Dupré equation to derive the adhesion energy of vesicles with known membrane tension.

Our results show that THD affects the adhesion of integrin-reconstituted vesicles to fibrinogen (Figure 1b) and induces integrin clustering (Figure 1c). The vesicles reach an adhesion energy to membrane tension ratio (W/σ ratio) of around 0.3 (Table 1, Figure 2). The W/σ ratio of integrin-containing protocells in the presence of Mn^{2+}/Mg^{2+} is slightly higher. This is expected as the density of active integrin molecules is 165 molecules/μm^2 after ion activation, compared to 149 after THD activation (Table 1).

It should be noted that our study shows for the first time integrin activation and clustering induced by THD in a cell-mimicking environment.[21] In particular, the observation that the activation of integrin by THD in combination with the binding of integrin to the substrate leads to integrin clustering, represents a valuable finding because the exact role of talin in the formation of integrin clusters is still unknown.[22]

Besides the possibility to produce GUVs with highly defined constituents, our study establishes a basis to co-reconstitute multiple transmembrane proteins into GUVs in appropriate proportions. This is particularly interesting for the investigation of interactions between multiple transmembrane proteins and for the development of complex synthetic cells. For example, both talin and kindlin bind to the cytoplasmic domains of integrin beta subunits and yet the molecular mechanisms of such interplay among these proteins for integrin activation are largely unknown. Using our synthetic approach, it will be possible to elucidate current simulation results[21] on how kindlin and talin cooperate in the activation of $\alpha_{IIb}\beta_3$ integrins. Furthermore, the integrin–THD complexes presented in this work are highly modular and may be used in combination with optogenetic tools[23] as a template to study the switch of molecular force transmission during adhesion.

The controlled molecular density of integrin–THD complexes in the vesicle membrane gives also the possibility to modulate, from the inside, the number of integrin bonds formed at the cell-extracellular interface. Such setup could be combined with extracellular nanopatterning of integrin ligands, as we have done in previous studies[24a,24b] to define how the local variations of integrin binding at the nanoscale are further regulated by integrin THD complex densities.

In terms of specificity of integrin binding, our synthetic cell biology approach to mimic integrin-mediated adhesion is suitable to be combined with ligands for RGD-binding integrins, such as those reviewed in Kapp et al.[25] By controlling the binding affinity of the ligands toward specific integrin subtypes, it is possible to selectively activate or block integrins. Combining these compounds with the synthetic cell system presented here will be of great advantage to define the distinct contribution of integrin conformational transitions and clustering on the half-maximal inhibitory concentration (IC_{50}) values, which so far showed variability when comparing cell-free ELISA-based systems with in vitro cell culture setup.

In conclusion, this study presents a mimicry of the inside–out activation of integrin via THD in cell-sized liposomes. The adhesion of integrin-containing protocells to fibrinogen increases with an increasing THD:integrin ratio, i.e., increasing integrin–THD complex density. The formation of these protocells was possible by a technique based on droplet-based microfluidics that allows us to precisely define the composition of the GUV. This work is an example of the formation of complex and functional synthetic cells. It provides new perspectives for mimicking complex protein–protein interactions for quantitative adhesion studies, for example, the dynamics of protein–protein interactions in the assembly, disassembly, and regulation of adhesion structures in synthetic cells. The formation of such model systems provides the means to investigate additional protein-protein interactions within a cell-mimicking environment. This is a necessary step toward the assembly of functional and complex synthetic cells.

4. Experimental Section

Cloning Expression and Purification of mTalin Head Domain: Mouse talin head domain (1-405) was expressed using pHMT29 vector (based on pET151-TOPO from ThermoFisher) encoding an N-terminal His tag followed by TEV cleavage site. A 7.5 L culture of *E. coli* BL21(DE3) was induced with 200 μM isopropyl-beta-D-thiogalactopyranoside (IPTG) and grown at 15 °C overnight. The cells were harvested and lysed by sonication in lysis buffer (50 mM Tris pH 8, 0.5 M NaCl, 20 mM Imidazole, 1 mM dithiothreitol (DTT)) containing 0.2 mg mL^{-1} lysozyme, 20 μg mL^{-1} DNase, 1 mM MgCl$_2$, 1 mM phenylmethylsulfonyl fluoride (PMSF) and protease inhibitor cocktail. After clarification by centrifugation, the lysate was applied to a Ni column (HisTrap_FF_crude_5ml, GE Healthcare) equilibrated and washed with lysis buffer. Talin was eluted from the column in one step with the same buffer containing 0.5 M imidazole and applied directly to a size exclusion (SEC) column (HiLoad_16/60_Superdex200 prep-grade, GE Healthcare) equilibrated with 50 mM Tris pH 8, 100 mM NaCl, and 1 mM DTT. The protein migrating as a single peak at 70 mL was pooled. Part of the protein was subject to TEV cleavage overnight at 4 °C followed by rebinding on a Ni column. The flow through from the Ni column, containing the cleaved protein without His tag was collected. The remaining protein from the SEC separation was applied to a cation exchange column (Tricorn Mono S 10/100_GL, GE Healthcare) equilibrated with 50 mM Hepes pH 6.7. The bound talin was eluted from the column with a gradient to 1 M NaCl yielding pure His-talin head domain.

Purification and Labelling of Integrin $\alpha_{IIb}\beta_3$: Integrin $\alpha_{IIb}\beta_3$ was purified from detergent extracts of human platelets (received from Katharinenhospital Stuttgart, Germany) by affinity chromatography via Concanavalin A and Heparin columns (both GE Healthcare, UK) followed by size exclusion chromatography (Superdex 200 pg; GE Healthcare, UK)

**ADVANCED
SCIENCE NEWS**

www.advancedsciencenews.com

**ADVANCED
NANOBIOMED
RESEARCH**
Open Access

www.advnanobiomedres.com

as described previously.[13] The purity of the protein was confirmed by SDS-PAGE and western blotting (antibody against integrin α_{IIb} subunit (clone #745201, MAB7616, R&D Systems, USA) and antibody against integrin β_3 subunit (clone PM6/13, CBL479, Merck Millipore, USA)).

For labeling, the integrin was rebuffered from storage buffer (20 mM Tris-HCl (Carl Roth, Germany) pH 7.4, 150 mM NaCl (Carl Roth, Germany), 1 mM $CaCl_2$ (*$2H_2O$, Calbiochem, USA), 1 mM $MgCl_2$ (*$6H_2O$, Applichem, Germany), 0.1% (w/v) Triton X-100 (Carl Roth, Germany), 0.02% (w/v) NaN_3 (Sigma-Aldrich, USA)) into phosphate-buffered saline (PBS, Gibco, USA) by dialysis and incubated with a 70× molar excess of Alexa Fluor™ 568N-hydroxysuccinimide (NHS) ester (ThermoFisher, USA) for 1 h on ice. The reaction was quenched by a 100× molar excess of Tris-HCl pH 7.4. Next, excessive reagent was eliminated and the labeled integrin rebuffered to storage buffer via a centrifugal filter unit (MWCO 100 kDa). The dye/protein ratio of 6.1 was determined by absorbance measurements at OD_{578} (dye extinction factor: 91 300 $mol^{-1} cm^{-1}$; correction factor of dye at OD_{280}: 0.46).

Reconstitution of Integrin $\alpha_{IIb}\beta_3$ into Liposomes: Integrin $\alpha_{IIb}\beta_3$ was reconstituted into lipid vesicles according to a procedure described elsewhere.[15b] First, the phospholipid L-α-phosphatidylcholine from chicken egg (egg PC, Avanti Polar Lipids, USA) was dried under a nitrogen stream and remaining traces of solvent were removed overnight under vacuum. The dried lipids were solubilized to a total lipid concentration of 870 µM in buffer (20 mM Tris-HCl pH 7.4, 50 mM NaCl, 1 mM $CaCl_2$ and 0.1% (w/v) Triton X-100) containing 1 µM integrin $\alpha_{IIb}\beta_3$ and incubated at 37 °C for 2 h. Subsequently, Triton X-100 was removed by incubating the mixture twice for 3.5 h at room temperature with 50 mg mL^{-1} Bio-Beads SM-2 (BioRad, USA). The Bio-Beads were washed with methanol and water as described by Holloway.[26] Prepared proteoliposomes were stored at 4 °C and used within 24 h after production.

Preparation of Large Unilamellar Vesicle: For the formation of LUVs, the lipids 1,2-dioleoyl-sn-glycero-3-phosphocholine (DOPC) and 1,2-dioleoyl-3-trimethylammonium-propane (DOTAP) were obtained from Avanti (Avanti Polar Lipids, USA) and ATTO488-labeled 1,2-dioleoyl-sn-glycero-3-phosphoethanolamine (DOPE) was obtained from ATTO TEC (Siegen, Germany).

LUVs were produced according to previously reported protocols.[27] First, the desired lipid composition was mixed, gently N_2-dried, and evaporated for 1–2 h to remove the remaining chloroform. The resulting lipid film was rehydrated by 20 s vortexing in Milli-Q water (Millipore filtered) to a final concentration of 3 mM. The LUVs used for the integrin clustering experiment were composed of 2:8 DOTAP:DOPC, the LUVs for all other adhesion experiments were composed of 20:79.5:0.5 DOTAP:DOPC:ATTO488-DOPE. To achieve homogeneous liposome size, the solution was pushed through a polycarbonate filter with 50 nm pore size (Whatman, Germany) 7 times using an extruder (Avanti Polar Lipids, USA). The mean diameter of the resulting LUVs was determined by dynamic light scattering (DLS) to be 100 ± 15 nm. The LUV solution was kept up to 48 h at 4 °C in the dark.

Assembly of Integrin and THD Containing Protocells: All protocells in this study were produced based on a recently published protocol.[13] For the formation of protein-containing vesicles, 1.2 mM lipids (proteoliposomes: bare LUVs 1:9, resulting in 330 integrins μm^{-2} of the total lipid bilayer area) premixed with 2, 10, 30, 80, 200, or 1000 nM THD in 20 mM Tris-HCl pH 7.4, 50 mM NaCl, 1 mM $CaCl_2$, and 20 mM sucrose (Acros Organics, USA) were encapsulated into monodisperse water-in-oil droplets (Figure 1a,I).

As a control, integrin-containing vesicles without THD or alternatively with 1 mM $MnCl_2$ (*$4H_2O$, Carl Roth, Germany)/1 mM $MgCl_2$ were produced. In addition, integrin-free protocells with 200 nM THD or 1 mM $MnCl_2$/1 mM $MgCl_2$ were created by replacing the proteoliposomes with bare LUVs composed of egg PC.

The microfluidic droplets were created in devices made of PDMS (Sylgard 184, Dow Corning, USA) on glass coverslips (Carl Roth, Germany). Photo- and soft-lithography methods[28] were used for their preparation as described previously.[29] For the charge-mediated formation of dsGUVs the oil phase consisted of FC-40 fluorinated oil (3M, USA) with 1 mM of the block-copolymer surfactant

perfluoropolyether (PFPE) (7000 g mol^{-1})-polyethylenglycol (PEG) (1400 g mol^{-1})-PFPE (7000 g mol^{-1}) (TRI7000) synthesized according to protocols published earlier[29,30] and ≈10 mM PFPE-carboxylic acid (Krytox, MW 7000–7500 g mol^{-1}; DuPont, Germany).[31] The droplets were created at 1 kHz with a diameter of 30 µm by using syringe pumps (PUMP 11 ELITE; Harvard apparatus, USA). Each sample was prepared from 70 µl aqueous phase.

The required lipid concentration to obtain a continuous bilayer at the droplets' interface was calculated according to Weiss et al.[13] For the production of dsGUVs (Figure 1a,II) with a diameter of 30 µm, a lipid concentration of 950 µM is necessary. In this study, an excess of lipids was used to guarantee a continuous bilayer and to counteract some loss of lipids during preparation.

The created dsGUVs were transferred from the droplet-stabilizing containers into a physiologically relevant environment by a previously described bulk release method (Figure 1a,III).[13] 50 µl of one of the following buffers was added. For THD-containing vesicles and the controls: 20 mM Tris-HCl pH 7.4, 50 mM NaCl, 1 mM $CaCl_2$, and 20 mM D-(+)-glucose (Sigma-Aldrich, Germany); for the $MnCl_2$/$MgCl_2$ containing vesicles the same buffer supplemented with 1 mM $MnCl_2$ and 1 mM $MgCl_2$. 70 µl of 30 vol% perfluoro-1-octanol destabilizing surfactants (Sigma-Aldrich, Germany) dissolved in FC-40 oil was added to the droplet emulsion to finally release the protocells into the appropriate buffer solution. The released GUVs (Figure 1a,IV) were used for adhesion and integrin-clustering experiments (Figure 1a,V). Their bending rigidity was assessed from fluctuation analysis.[32]

Experimental Setup for Adhesion Studies: The adhesion properties of the protocells were investigated on fibrinogen-coated glass surfaces. To this end, plasma-treated (O_2 plasma, 200 W, 60 s) glass coverslips (Carl Roth, Germany) were incubated with 0.1 mg mL^{-1} fibrinogen (Merck Millipore, Germany) in PBS solution (8.5 µg cm^{-2}) at 4 °C overnight. The fibrinogen-coated slides were rinsed three times with PBS directly before use and once with the appropriate buffer solution containing 20 mM glucose. 30 µL of the protocell solution was transferred on to the fibrinogen-coated slide between two spacers made up of double-sided sticky tape (Tesa, Germany, thickness ≈80 µm) and a lid consisting of a coverslip (Carl Roth, Germany). To avoid evaporation of the liquid and disruptive flux, the sample-containing chamber was closed by two-component glue (Twinsil, Picodent GmbH, Germany). To allow the vesicles to settle down and interact with the protein-coating, the samples were kept overnight at 4 °C in the dark prior to adhesion analysis.

Microscopy: All fluorescence images were taken using a Leica SP5 microscope (Leica Microsystems GmbH, Germany) with a 63× oil objective (HCX PL APO 63×/1.40-0.60; Leica Microsystems GmbH, Germany). The fluorophores were excited by a white light laser at 488 nm (ATTO488) and 568 nm (Alexa568) and detected in a window between 498–540 nm and 578–630 nm, respectively. The pinhole for data acquisition was set to 1 Airy unit (96 µm Airy disk diameter of 0.9 µm thickness of the optical slice).

RICM images were taken with an inverted microscope (Zeiss). To produce coherent, monochromatic light ($\lambda = 555$ nm), a RICM filter cube, a beam splitter (50R/50T VIS), two polarization filters (AHF, Germany), and an LED light source (Zeiss, Germany) were used. The sample was observed through a 63× Plan Neofluar Antiflex oil immersion objective (NA 1.25) (Zeiss, Germany). Image analysis was performed using ImageJ and Fiji.

Statistical Analysis: All values are expressed as mean +/− SEM (standard error of the mean), if not stated differently. Sample sizes (n) are described in the figure/table captions. For clustering analysis, an unpaired, two-tailed student's t-test assuming a Gaussian distribution tested by D'Agostino and–Pearson normality test (normality defined for $p > 0.05$) was performed using GraphPad Prism version 9.3.1. Significance was defined as $p \leq 0.05$.

Supporting Information

Supporting Information is available from the Wiley Online Library or from the author.

Acknowledgements

Conflict of Interest

The authors declare no conflict of interest.

Author Contributions

L.T.B.: performed all experiments and wrote the manuscript; A.S.B.: integrin-labeling, proteoliposomes, clustering analysis, contributed to manuscript writing; E.A.C.-A.: integrin adhesion analysis and discussion; R.B.L., R.D.: Fluctuation and FRAP analysis; B.G.: THD production, design of experiment, contributed to the writing of manuscript: R.L.: experimental analysis, design of experiment, contributed to manuscript writing; J.P.S.: general design of experiment, manuscript writing, supervision.

Data Availability Statement

The data that support the findings of this study are available from the corresponding author upon reasonable request.

Keywords

[1] a) C. Wu, *Cell Adhes. Migr.* **2007**, *1*, 13; b) A. L. Berrier, K. M. Yamada, *J. Cellular Physiol.* **2007**, *213*, 565.

[2] a) B. Wehrle-Haller, B. Imhof, *Trends Cell Biol.* **2002**, *12*, 382; b) B. Geiger, A. Bershadsky, R. Pankov, K. M. Yamada, *Nat. Rev. Mol. Cell Biol.* **2001**, *2*, 793; c) J. Qin, O. Vinogradova, E. F. Plow, *PLOS Biol.* **2004**, *2*, 169; d) C. Cluzel, F. Saltel, J. Lussi, F. Paulhe, B. A. Imhof, B. Wehrle-Haller, *J. Cell Biol.* **2005**, *171*, 383.

[3] a) I. D. Campbell, M. J. Humphries, *Cold Spring Harbor Perspectives Biol.* **2011**, *3*, a004994; b) M. H. Ginsberg, *BMB Rep.* **2014**, *47*, 655;
c) S. J. Shattil, C. Kim, M. H. Ginsberg, *Nat. Rev. Mol. Cell Biol.* **2010**, *11*, 288; d) S. H. Lo, *Dev. Biol.* **2006**, *294*, 280.

[4] a) R. Li, N. Mitra, H. Gratkowski, G. Vilaire, R. Litvinov, C. Nagasami, J. W. Weisel, J. D. Lear, W. F. DeGrado, J. S. Bennett, *Science* **2003**, *300*, 795; b) S. Miyamoto, S. K. Akiyama, K. M. Yamada, *Science* **1995**, *267*, 883; c) T. Hato, N. Pampori, S. J. Shattil, *J. Cell Biol.* **1998**, *141*, 1685.

[5] a) S. J. Shattil, P. J. Newman, *Blood* **2004**, *104*, 1606; b) F. Ye, C. Kim, M. H. Ginsberg, *Blood* **2012**, *119*, 26; c) R. O. Hynes, *Cell* **2002**, *110*, 673; d) B. S. Coller, S. J. Shattil, *Blood* **2008**, *112*, 3011; e) S. J. Shattil, H. Kashiwagi, N. Pampori, *Blood* **1998**, *91*, 2645; f) G. A. Marguerie, E. F. Plow, T. S. Edgington, *J. Biol. Chem.* **1979**, *254*, 5357; g) M. Kloczewiak, S. Timmons, T. J. Lukas, J. Hawiger, *Biochemistry* **1984**, *23*, 1767; h) J. S. Bennett, *Ann. N Y Acad. Sci.* **2001**, *936*, 340.

[6] J. P. Frohnmayer, D. Brüggemann, C. Eberhard, S. Neubauer, C. Mollenhauer, H. Boehm, H. Kessler, B. Geiger, J. P. Spatz, *Angew. Chem., Int. Ed.* **2015**, *54*, 12472.

[7] R. Zarka, M. B. Horev, T. Volberg, S. Neubauer, H. Kessler, J. P. Spatz, B. Geiger, *Nano Lett.* **2019**, *19*, 1418.

[8] a) K. Zhang, J. Chen, *Cell Adhes. Migr.* **2012**, *6*, 20; b) A. Cierniewska-Cieslak, C. S. Cierniewski, K. Bledzka, M. Papierak, L. Michalec, L. Zhang, T. A. Haas, E. F. Plow, *J. Biol. Chem.* **2002**, *277*, 11126; c) B. Leitinger, A. McDowall, P. Stanley, N. Hogg, *Biochim. Biophys. Acta* **2000**, *1498*, 91; d) J. Takagi, B. M. Petre, T. Walz, T. A. Springer, *Cell* **2002**, *110*, 599; e) J. Gailit, E. Ruoslahti, *J. Biol. Chem.* **1988**, *263*, 12927.

[9] a) F. Ye, G. Hu, D. Taylor, B. Ratnikov, A. A. Bobkov, M. A. McLean, S. G. Sligar, K. A. Taylor, M. H. Ginsberg, *J. Cell Biol.* **2010**, *188*, 157; b) P. R. Elliott, B. T. Goult, P. M. Kopp, N. Bate, J. G. Grossmann, G. C. Roberts, D. R. Critchley, I. L. Barsukov, *Structure* **2010**, *18*, 1289; c) D. A. Calderwood, R. Zent, R. Grant, D. J. Rees, R. O. Hynes, M. H. Ginsberg, *J. Biol. Chem.* **1999**, *274*, 28071; d) D. A. Calderwood, B. Yan, J. M. de Pereda, B. G. Alvarez, Y. Fujioka, R. C. Liddington, M. H. Ginsberg, *J. Biol. Chem.* **2002**, *277*, 21749; e) S. Tadokoro, S. J. Shattil, K. Eto, V. Tai, R. C. Liddington, J. M. de Pereda, M. H. Ginsberg, D. A. Calderwood, *Science* **2003**, *302*, 103; f) G. Giannone, G. Jiang, D. H. Sutton, D. R. Critchley, M. P. Sheetz, *J. Biol. Chem.* **2003**, *163*, 409; g) H. Priddle, L. Hemmings, S. Monkley, A. Woods, B. Patel, D. Sutton, G. A. Dunn, D. Zicha, D. R. Critchley, *J. Cell Biol.* **1998**, *142*, 1121.

[10] a) T. A. Bunch, *J. Biol. Chem.* **2010**, *285*, 1841; b) S. J. Ellis, E. Lostchuck, B. T. Goult, M. Bouaouina, M. J. Fairchild, P. Lopez-Ceballos, D. A. Calderwood, G. Tanentzapf, *PLoS Genet.* **2014**, *10*, 1004756.

[11] B. G. Petrich, P. Marchese, Z. M. Ruggeri, S. Spiess, R. A. M. Weichert, F. Ye, R. Tiedt, R. C. Skoda, S. J. Monkley, D. R. Critchley, M. H. Ginsberg, *J. Exp. Med.* **2007**, *204*, 3103.

[12] a) N. J. Anthis, K. L. Wegener, F. Ye, C. Kim, B. T. Goult, E. D. Lowe, I. Vakonakis, N. Bate, D. R. Critchley, M. H. Ginsberg, I. D. Campbell, *EMBO J.* **2009**, *28*, 3623; b) K. L. Wegener, A. W. Partridge, J. Han, A. R. Pickford, R. C. Liddington, M. H. Ginsberg, I. D. Campbell, *Cell* **2007**, *128*, 171; c) E. Goksoy, Y. Q. Ma, X. Wang, X. Kong, D. Perera, E. F. Plow, J. Qin, *Mol. Cell* **2008**, *31*, 124; d) B. Garcia-Alvarez, J. M. de Pereda, D. A. Calderwood, T. S. Ulmer, D. Critchley, I. D. Campbell, M. H. Ginsberg, R. C. Liddington, *Mol. Cell* **2003**, *11*, 49.

[13] M. Weiss, J. P. Frohnmayer, L. T. Benk, B. Haller, J. W. Janiesch, T. Heitkamp, M. Borsch, R. B. Lira, R. Dimova, R. Lipowsky, E. Bodenschatz, J. C. Baret, T. Vidakovic-Koch, K. Sundmacher, I. Platzman, J. P. Spatz, *Nat. Mater.* **2018**, *17*, 89.

[14] a) O. Biner, T. Schick, Y. Muller, C. von Ballmoos, *FEBS Lett.* **2016**, *590*, 2051; b) R. B. Lira, T. Robinson, R. Dimova, K. A. Riske, *Biophys. J.* **2019**, *116*, 79.

[15] a) S. Goennenwein, M. Tanaka, B. Hu, L. Moroder, E. Sackmann, *Biophys. J.* **2003**, *85*, 646; b) E. M. Erb, K. Tangemann, B. Bohrmann, B. Muller, J. Engel, *Biochemistry* **1997**, *36*, 7395.

[16] B. Yan, D. A. Calderwood, B. Yaspan, M. H. Ginsberg, *Biol. Chem.* **2001**, *276*, 28164.

[17] a) P. B. Contino, C. A. Hasselbacher, J. B. Ross, Y. Nemerson, *Biophys. J.* **1994**, *67*, 1113; b) E. Reimhult, B. Kasemo, F. Hook, *Int. J. Mol. Sci.* **2009**, *10*, 1683; c) G. Puu, I. Gustafson, *Biochim. Biophys. Acta* **1997**, *1327*, 149.

[18] M. Gleisner, B. Kroppen, C. Fricke, N. Teske, T. T. Kliesch, A. Janshoff, M. Meinecke, C. Steinem, *Biol. Chem.* **2016**, *291*, 19953.

[19] M. E. Schrader, *Langmuir* **1995**, *11*, 3585.

[20] A. Albersdorfer, T. Feder, E. Sackmann, *Biophys. J.* **1997**, *73*, 245.

[21] Z. Haydari, H. Shams, Z. Jahed, M. R. K. Mofrad, *Biophys. J.* **2020**, *118*, 1977.

[22] T. N. Durrant, M. T. van den Bosch, I. Hers, *Blood* **2017**, *130*, 1607.

[23] B. Yu, W. Tabis, I. Bialo, F. Yakhou, N. B. Brookes, Z. Anderson, Y. Tang, G. Yu, M. Greven, *Phys. Rev. X* **2020**, *10*, 021059.

[24] a) M. Arnold, E. A. Cavalcanti-Adam, R. Glass, J. Blummel, W. Eck, M. Kantlehner, H. Kessler, J. P. Spatz, *Chemphyschem* **2004**, *5*, 383; b) E. A. Cavalcanti-Adam, T. Volberg, A. Micoulet, H. Kessler, B. Geiger, J. P. Spatz, *Biophys. J.* **2007**, *92*, 2964.

[25] T. G. Kapp, F. Rechenmacher, S. Neubauer, O. V. Maltsev, E. A. Cavalcanti-Adam, R. Zarka, U. Reuning, J. Notni, H. J. Wester, C. Mas-Moruno, J. Spatz, B. Geiger, H. Kessler, *Sci. Rep.* **2017**, *7*, 39805.

[26] P. W. Holloway, *Analyt. Biochem.* **1973**, *53*, 304.

[27] a) J. M. Johnson, T. Ha, S. Chu, S. G. Boxer, *Biophys. J.* **2002**, *83*, 3371; b) C. Herold, G. Chwastek, P. Schwille, E. P. Petrov, *Langmuir* **2012**, *28*, 5518.

[28] a) H. Gu, M. H. Duits, F. Mugele, *Int. J. Mol. Sci.* **2011**, *12*, 2572; b) Y. Xia, G. M. Whitesides, *Annu. Rev. Mater. Sci.* **1998**, *28*, 153.

[29] I. Platzman, J. W. Janiesch, J. P. Spatz, *J. Am. Chem. Soc.* **2013**, *135*, 3339.

[30] J. W. Janiesch, M. Weiss, G. Kannenberg, J. Hannabuss, T. Surrey, I. Platzman, J. P. Spatz, *Anal. Chem.* **2015**, *87*, 2063.

[31] B. Haller, K. Jahnke, M. Weiss, K. Göpfrich, I. Platzman, J. P. Spatz, *Adv. Intell. Syst.* **2021**, *3*, 2000190.

[32] a) R. S. Gracià, N. Bezlyepkina, R. L. Knorr, R. Lipowsky, R. Dimova, *Soft Matter* **2010**, *6*, 1472; b) H. A. Faizi, C. J. Reeves, V. N. Georgiev, P. M. Vlahovska, R. Dimova, *Soft Matter* **2020**, *16*, 8996.